Desalination and Water Treatment
www.deswater.com

doi:10.5004/dwt.2019.23548

156 (2019) 117–125
July

Performance evaluation of PVT-CPC integrated solar still under natural circulation

Kuber Nath Mishra[a,*], Md. Meraj[b], Anil Kr. Tiwari[a], G.N. Tiwari[c,d]

[a]*Department of Mechanical Engineering, National Institute of Technology Raipur, 492010, India, Tel. +918608471148, email: knmishra.phd2017.mech@nitrr.ac.in (K.N. Mishra), anil.kr.tiwari@gmail.com (A.K. Tiwari)*
[b]*Department of Mechanical Engineering, Jamia Millia Islamia, New Delhi, 110025, India, Tel. +919897965833, email: md.meraj1221@gmail.com (M. Meraj)*
[c]*Professor (Research) SRM University, Lucknow Deva Road, Lucknow (UP)*
[d]*Bag Energy Research Society (BERS), 11B, Gyan Khand 4,Indirapuram, Ghaziabad UP 201014, India, Tel. +919318466512, email: gntiwari@ces.iitd.ernet.in (G.N. Tiwari)*

Received 31 August 2018; Accepted 28 November 2018

ABSTRACT

Water purification through solar still offers the simplest and most cost-effective method of purifying contaminated water. The solar still yield is affected by climatic parameters and other design parameters like condensate cover angle, basin water depth, thermal insulation etc. To further enhance the condensate water yield, a compound parabolic concentrator integrated to the solar water still is utilized. In this paper, analytical expressions for basin water, cover glass temperature, and condensate water yield has been determined in terms of climatic and design parameters for the proposed fully covered photovoltaic thermal-compound parabolic concentrator (PVT-CPC) integrated solar still. The active solar still presented here works with natural mode of circulation. The analytical expressions for glass temperature (T_g), Water temperature (T_w), and basin temperature (T_b) have been derived on the basis of energy balance for top glass cover, water mass in the basin and basin liner respectively. Numerical analysis has been performed for climatic conditions of New Delhi and the climatic data is taken from the Indian Metrological Department (IMD), Pune, India. The temperature values obtained are used to compute the hourly yield, instantaneous thermal efficiency and overall thermal efficiency of the proposed active natural still with the help of MATLAB R2015a. Results are compared with conventional solar distillation system of same physical dimensions operating under same conditions. The proposed active natural still is found to yield 88.4% higher distilled water against the conventional still. Further, the conventional still is found to exhibit higher instantaneous thermal efficiency throughout the day with a peak value of 45.1% against 13.6% for proposed active still. Also, an overall thermal efficiency of 24.2% is obtained for conventional still compared to 9.8% for proposed active still.

Keywords: PVT-CPC; Active natural still; Solar energy; Natural circulation

1. Introduction

Water is the key factor for birth and evolution of life on Earth. With ever-increasing demand-supply gap for fresh water, a sustainable and renewable energy-based purification system is the only way forward to bridge this gap. The current global scenario of water scarcity can be attributed to the small share of fresh water available on our planet and to a greater extent can be a credited to the extremely fast-paced human development. The fresh

*Corresponding author.

Presented at the InDA Conference 2018 (InDACON-2018), 20-21 April 2018, Tiruchirappalli, India

water available has been converted to unusable form at a pace that has left many nations in a state of extreme scarcity and to look for desperate measures to conserve whatever water is left with them. The solution to the crisis lies in its conservation, reuse of water for more than one purpose and recycling. While the former two are socially dependent and can only be implemented by mass education, the latter is the only solution available to engineers. Over the decades the water recycling has evolved to a great extent and cities worldwide have in place water harvesting and sewage treatment systems to conserve and reuse water at large scale. At a relatively smaller scale, societies have adopted to conserve water in underground aquifers and tanks for later use. At the domestic level, membrane purification technologies have paved their way to most of the homes and commercial establishments globally. Though reverse osmosis (RO) being the most widely used water purification method today, has its own inherent drawbacks and limitations like every other technology. Intensive energy consumption and reject water disposal are a few of them. Harnessing renewable energy sources for water purification is a technology that has received its due attention in the last few decades and one such promising technology is water desalination through solar stills.

Solar stills operate without an externally connected energy source, are nonpolluting and provide clean water at zero operating cost of solar energy. The fundamentals of solar energy, still design modelling and its applications are presented by Tiwari [1] Though simple, robust and cost-effective, the solar stills are yet to be commercialized and developed to be a product as in case of RO technology due to its low daily yield. Ghobeity and Mitsos [2] have presented a detailed discussion of challenges in the design and implementation of solar desalination systems.

Giwa et al. [3] have reported the solution to make solar desalination competent with other technologies combined with other systems at a large scale. Pouyfaucon et al. [4] have concluded the best solar desalination solutions based upon the demand for water and a viable solution for developing markets for the solar still technology. Abdulkareem et al. [5] have elaborated a detailed study of recent progress in solar energy utilization for the purpose of water desalination and energy and economic efficiency of passive and active stills.

Tiwari and Sahota [6] have presented a review of the energy and economic efficiency of passive and active solar stills. Also, a detailed description of solar collectors and thermal modelling of active solar desalination systems is given by Tiwari and Sahota [7]. Tiwari and Tiwari [8–12] and Panchal and Patel [13] have reported various investigations to analyze the effect of different parameters on still performance. An investigation into the effect of water and airflow on CPC integrated concentric tubular solar water desalting system (CPC-CTSS) with a productivity improvement of 144% by the implementation of cold air and water flow over the condensing surface is reported by Arunkumar et al. [14]. A combination of solar stills with PVT collectors to improve daily yield has been reported by Mousa and Arabi [15]. They have investigated the performance improvement of a still coupled with a thermal collector and have reported the effect of parameters like glass cooling and forced circulation on the performance of the system.

A numerical simulation to analyze the combination of a CPC with a conventional still is performed and reported by Pearce and Denkenberger [16]. Deniz [17] has presented an energy and exergy efficiency of 48.1% and 2.76% for a flat plate collector coupled with a still. Poblete et al. [18] have highlighted the role of a reflector and basin temperature on the performance of a PVT combined with a solar still. An experimental investigation into the productivity enhancement of CPC tubular solar stills is reported by Arunkumar et al. [19]. Tripathi and Tiwari [20] have investigated the possibility of yield improvement through the development of an analytical expression for N-PVT-CPC to investigate the performance of N-PVT -CPC concentrators connected in series with a still.

2. System description

An active solar still under natural circulation mode coupled with a fully covered semitransparent photovoltaic thermal compound parabolic concentrator (PVT-CPC) as shown in Fig. 1a is investigated in this work.

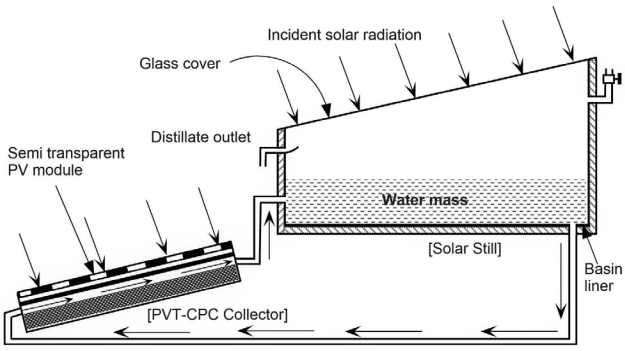

Fig. 1a. Schematic representation of (PVT-CPC) integrated solar still under natural circulation.

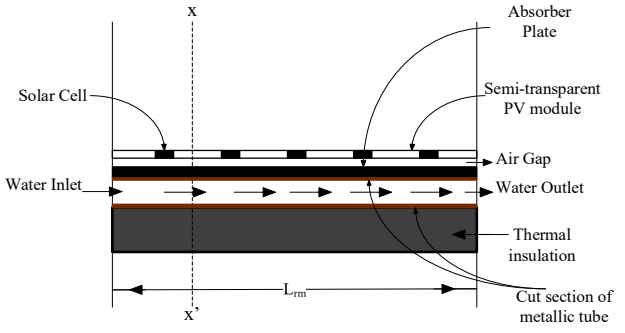

Fig. 1b. Sectional view of fully covered PVT-CPC collector.

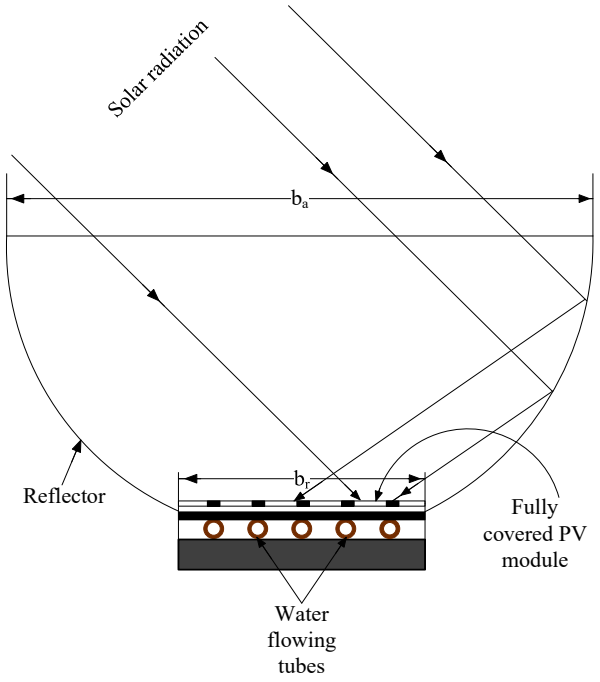

Fig. 1c. Detailed sectional front view of fully covered PVT-CPC collector system.

The PV integrated thermal collector with semitransparent PV module as the cover is combined to the solar still for active mode operation with natural mode of fluid circulation. The incident radiation reflected from the PVT concentrator falls on the collector area along with the direct incident radiation. The total area facing the incident radiation including reflected from CPC is assigned as aperture area (A_{apvt}) and the area of semitransparent PV module receiving the incident radiation is termed as receiver area (A_{rpvt}). The semitransparent module generates electrical energy while the radiation passing through the unpacked area of the module is gained by the absorber surface and the thermal energy is transferred to the water flowing in the tubes by natural circulation below the absorber plate of the PVT module. The temperature of the flowing water thus increases and this preheated water ensures the active mode operation of the still. In this manner, the fully covered PVT-CPC panel harnesses both the visible and infra-red spectrum of the sunlight for electrical and thermal energy. The electrical energy so obtained may be utilized for pump operation in forced circulation mode or any other suitable application. The performance characteristics of the above system are compared with a conventional single slope solar still without PVT collector with the same still dimensions under same operating conditions.

3. Methodology

The methodology adopted for carrying out the analysis is described in Fig. 2 .

3.1. Thermal modelling

Table 1
Design parameters

Parameter	Value	Parameter	Value
A_b	1 m²	$U_{sc,amb}$	9.17 W/m²K
A_{apvt}	4.2 m²	$U_{sc,abs}$	5.58 W/m²K
A_{rpv}	2.1 m²	h_w	100 W/m²
F'	0.97	h_i	2.8 W/m²
FF	0.88	α_{sc}	0.9
K_g	0.816 W/m K	α_{abs}	0.8
L_g	0.004 m	$U_{abs,amb}$	4.8 W/m²K
K_i	0.166 W/m K	PF_1	0.3783
L_i	0.100 m	PF_2	0.9213
K_{abs}	6 W/m K	β_{sc}	0.89
L_{abs}	0.002 m	τ_g	0.95
L_i	0.100 m	ρ	0.84
U_{L1}	3.47 W/m²K	α_g'	0.0095
U_{Lm}	7.62 W/m²K	α_w'	0.1787
U'_{Lm}	8.27 W/m²K	α_b'	0.5861
C_w	4200 J/kg K	M_w	50 kg
		V	4.11 m/s

3.1.1. Assumptions

For the purpose of simplification of the proposed analytical model, the following assumptions proposed by Tiwari et al. [21] were made to arrive at the energy balance equation of the still components

a. The average temperature of water in the solar still-basin and PVT-CPC is approximately same.
b. The heat capacity of solar cells, absorber, glass cover, reflector, and bottom insulation is neglected.
c. Solar still basin is always above the height of PVT-CPC for natural circulation mode.
d. One dimensional heat conduction is considered for the present modelling.
e. The present modelling is based upon quasi-steady state.
f. The ohmic losses for the semi-transparent PV module is neglected.

3.2 Energy balance of system components

3.2.1. Energy balance for the PVT-CPC collector

The energy balance for the PVT-CPC collector by Tiwari et al. [21] is presented as follows:

[Incident radiation on PVT collector] = [Heat loss from the solar cell to ambient from top surface] + [heat transferred from solar cell to absorber surface through glass] + [electrical energy generated by the PV cover]

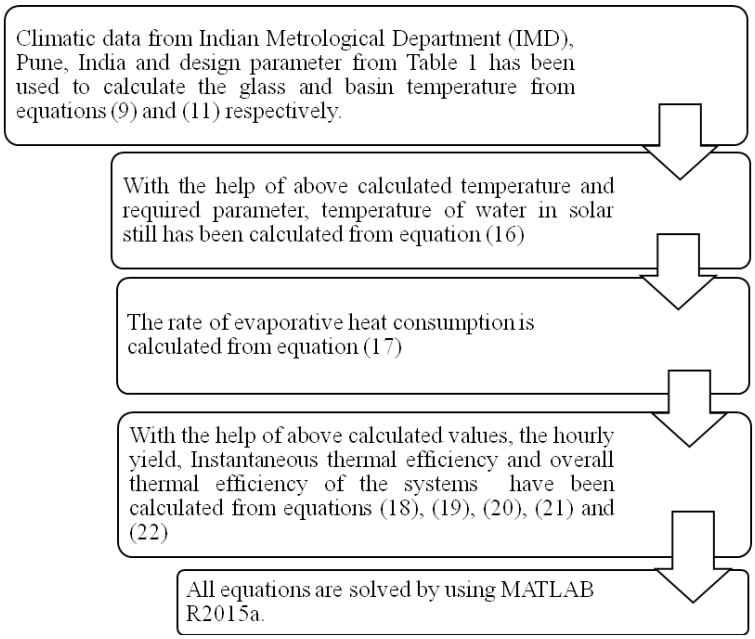

Fig. 2. Methodology adopted for the analysis.

$$\rho\alpha_{sc}\tau_g\beta_{sc}\eta I_U = U_{sc,amb}\left(T_{sc}-T_{amb}\right)A_{rpvt} + U_{sc,abs}\left(T_{sc}-T_{abs}\right)A_{rpvt} + \rho\eta_{sc}\tau_g\beta_{sc}I_U A_{apvt} \quad (1)$$

The corresponding PV cell temperature can be obtained from the above equation as

$$T_{sc} = \frac{(\alpha\tau)_{1,eff}\, I_u + U_{sc,amb}T_{amb} + U_{sc,abs}T_{abs}}{U_{sc,amb} + U_{sc,abs}} \quad (2)$$

3.2.2. Energy balance for PVT absorber surface

Amount of energy transferred to the absorber surface through unpacked area of the semi-transparent PV module is the difference of total incident radiation on receiver area A_{rpvt} and that converted to electrical energy through packed area of PV module.

$$\rho\alpha_c\tau_g^2\left(1-\beta_c\right)I_U A_{apvt} + U_{sc,amb}\left(T_{sc}-T_{amb}\right)A_{apvt} = F'h_{pf}\left(T_{abs}-T_w\right)A_{apvt} + U_{abs,amb}\left(T_{abs}-T_{amb}\right)A_{rpvt} \quad (3)$$

Absorber surface temperature can be obtained from the above equation as

$$T_{abs} = \frac{[(\alpha\tau)_{2,eff} + PF_1(\alpha\tau)_{1,eff}]I_U + U_{L2}T_{amb} + F'h_{pf}T_w}{U_{L2} + F'h_{pf}} \quad (4)$$

The temperature dependent electrical efficiency of the solar cell of the photovoltaic module is given by Evans [22]; Schott [23] and Tiwari et al. [24] as follows:

$$\eta_{sc} = \eta_0\left[1-\beta_0\left(T_{sc}-T_{amb}\right)\right] \quad (5)$$

Using Eqns. (1), (2) and (4), one can obtain the analytical expression of temperature dependent solar cell electrical efficiency for fully covered PVT-CPC collector operating under constant collection temperature mode as follows:

$$\eta_{sc} = \frac{\eta_0\left[1-\beta_0\left\{\dfrac{\begin{array}{c}\rho\alpha_{sc}\tau_g\beta_{sc}CI_u\left(F'h_{pf}+U_{L2}+PF_1U_{sc,abs}\right)+\left(U_{sc,abs}(\alpha\tau)_{2,eff}\,I_u\right)\\ +T_{amb}\left(F'h_{pf}U_{sc,amb}+U_{sc,amb}U_{L2}+U_{sc,abs}U_{L2}\right)\\ +F'h_{pf}U_{sc,abs}T_w-T_0\left(U_{sc,amb}+U_{sc,abs}\right)\left(F'h_{pf}+U_{L2}\right)\end{array}}{\left(U_{sc,amb}+U_{sc,abs}\right)\left(F'h_{pf}+U_{L2}\right)}\right\}\right]}{\left[1-\dfrac{\eta_0\beta_0\rho\tau_g\beta_cCI_u\left(F'h_{pf}+U_{L2}+PF_1U_{t,cp}\right)}{\left(U_{sc,amb}+U_{sc,abs}\right)\left(F'h_{pf}+U_{L2}\right)}\right]} \quad (6)$$

Now, using Eq. (6), the electrical efficiency and energy of PV module of fully covered PVT-CPC collectors can be estimated as follows:

$$\eta_m = \tau_g\beta_{sc}\eta_{sc} \quad (7a)$$

and,

$$\dot{E}_{el} = \eta_m\rho A_{apvt}I_u \quad (7b)$$

Further, following Tiwari [1], the energy balance equation for glass cover of solar still can be written as follows:

3.3. Energy balance for glass cover of still

[The incident solar radiation over glass + equivalent heat transfer from water to glass] = [Heat loss from glass to ambient by convection]

$$\alpha_g'I(t) + h_{1w}\left(T_w-T_g\right) = h_2\left(T_g-T_{amb}\right) \quad (8)$$

From the above Eq. (8), the equation for temperature of the glass is obtained as follows:

$$T_g = \frac{\alpha' I(t) + h_{1w}T_w + h_2 T_{amb}}{(h_{1w} + h_2)} \quad (9)$$

3.4. Energy balance for still basin liner

The net energy as absorbed by the basin can be presented as the sum of the heat transferred to basin water and heat loss through bottom insulation.

$$\alpha_b' I(t) = h_{1w}(T_b - T_w) + h_b(T_b - T_{amb}) \quad (10)$$

From Eq. (10). the expression for temperature of the basin is obtained as follows:

$$T_b = \frac{\alpha_b' I(t) + T_w h_{1w} + h_b T_{amb}}{h_{1w} + h_b} \quad (11)$$

3.5. Energy balance equation for water mass passing through active still

$$\dot{Q}_u + h_3(T_b - T_w) = M_w C_w \frac{dT_w}{dT} + h_w(T_w - T_g) \quad (12)$$

Where $\dot{Q}_u$ is the useful heat gain due to PVT-CPC as given by Tiwari et al. [21] as follows:

$$\dot{Q}_u = A_{rpvt} F_{pvt}[PF_2(\alpha\tau)_{meff} I_u - U_{lm}(T_w - T_{amb}) \quad (13)$$

The resultant equation in the following form can be obtained as follows:

$$\frac{dT_w}{dt} + aT_w = af(t) \quad (14)$$

where $a = \frac{U + (UA)_{eff}}{M_w C_w}$

and

$$f(t) = \frac{\alpha_{eff} I(t) + (\alpha\tau)_{eff} I_u + (U + (UA)eff)T_{amb}}{M_w C_w} \quad (15)$$

on solving the differential Eq. (14), the temperature of water in the solar still is obtained as

$$T_w = \frac{f(t)}{a}\left[1 - \exp(-a\Delta t)\right] + T_{W0}\exp(-a\Delta t) \quad (16)$$

where T_{W0} is temperature of basin water at $t = 0$ and $\overline{f(t)}$ is average value of f(t) for time interval 0 to t.

The rate of heat consumption in evaporation and hourly yield can be obtained from

$$\dot{q}_{ew} = h_{ew}(T_w - T_g) \quad (17)$$

$$m_{ew} = \frac{h_{ew}(T_w - T_g)}{l} X\, 3600\, kg/m^2 \quad (18)$$

Further, the instantaneous thermal efficiency for conventional solar still (when, $\dot{Q}_u = 0$) can be obtained as follows:

$$\eta_{i,conventional} = \frac{\dot{q}_{ew}}{I(t)} \quad (19)$$

The instantaneous thermal efficiency for active solar still under natural mode can be obtained as follows:

$$\eta_{i,active,natural} = \frac{\dot{q}_{ew}}{I(t) + I_u A_{apvt}} \quad (20)$$

The overall daily thermal efficiency for the conventional solar still with unit area under natural mode for the sunshine period between 8:00 h to 17:00 h can be obtained as follows:

[Overall daily thermal efficiency] = [Sum total of heat consumption in evaporation for 24 h] / [Sum total of incident radiation on still for sunshine hours]

$$\eta_{o,conventional} = \frac{\sum_{i=1}^{24} \dot{q}_{ew}}{\sum_{i=1}^{10} I(t)} \quad (21)$$

Also, the overall daily thermal efficiency for the active solar still under natural mode for sunshine period between 8:00 h to 17:00 h can be obtained as follows:

[Overall daily thermal efficiency] = [Sum total of heat consumption in evaporation for 24 h] / [Sum total of incident radiation on still for sunshine hours] + [(Sum total of incident radiation on PVT-CPC collector for sunshine hours) X (Aperture area of PVT-CPC collector)]

$$\eta_{o,active,natural} = \frac{\sum_{i=1}^{24} \dot{q}_{ew}}{\sum_{i=1}^{10} I(t) + \sum_{i=1}^{10} A_{apvt} I(t)} \quad (22)$$

The unknown expressions in the above model are given in the Appendix.

4. Results and discussion

The discussion over the results obtained by the analysis are presented under the following heads:

4.1. Climatic and environmental parameters

Hourly variation of incident solar radiation and ambient temperature for a typical day of the month of March for New Delhi is shown in Fig. 3. The highest ambient temperature of 28.9°C occurs at 17:00 h for a corresponding incident radiation of 285.21 W/m^2 though the highest incident radiation of 933.33 W/m^2 is recorded at 13:00 h.

4.2. Electrical power output from semitransparent PV module of PVT-CPC collector

The PVT-CPC integrated with solar still is fully covered with a semitransparent PV module that generates electrical power. The PV module is integrated into the PVT collector as shown in Fig. 1a, 1b, and 1c. The packed area of the module generates electrical power while the unpacked area permits the thermal energy to the collector absorber and hence to the water flowing into the tubes. Hourly variation of electrical power output from this module is presented in Fig. 4. The Peak power output of 272.2 W is obtained at noon hours

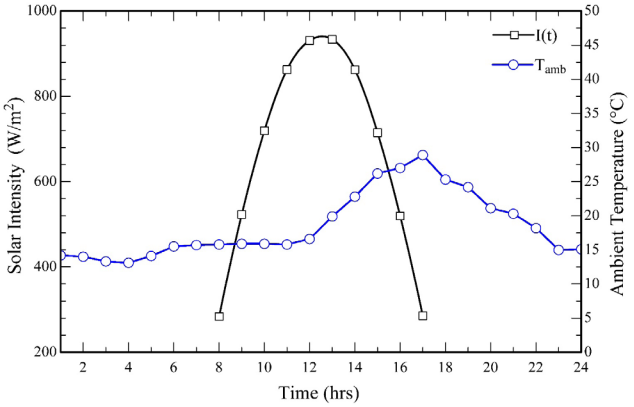

Fig. 3. Hourly variation of incident solar radiation and ambient temperature.

while the minimum energy output is obtained at 8:00 h and 17:00 h corresponding to minimum incident radiation.

4.3. PV module efficiency with respect to cell temperature

Fig. 5 Shows hourly variation of electrical efficiency of semitransparent PV module covering the PVT system for corresponding cell temperatures. The relation between the electrical performance of a PV cell and temperature is a well-established phenomenon and the results shown for this case agree with the previous reported literature [25]. The peak electrical efficiency is found to be 14.3% occurring at 8:00 h corresponding to an incident radiation value of 283.9 W/m² and a cell temperature of 39.7°C whereas the minimum efficiency is calculated to be 9.9% occurring at 13:00 h for a corresponding maximum incident radiation of 933.33 W/m² and a resultant cell temperature of 104.6°C. The changes in irradiation directly affect the short-circuit and output current of the solar cell junctions [25]. The output voltage of the PV modules decreases drastically with rise in ambient temperature.

4.4. Temperature variation in still components

A graphical representation of the hourly temperature variation of still components for the proposed active natural and conventional systems is presented in Fig. 6. The curves

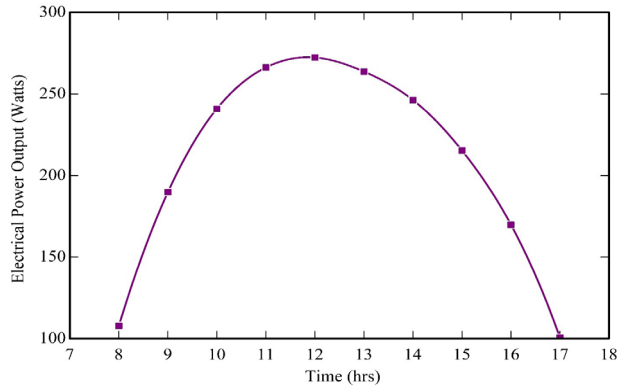

Fig. 4. Hourly variation of electrical power output from semitransparent PV module.

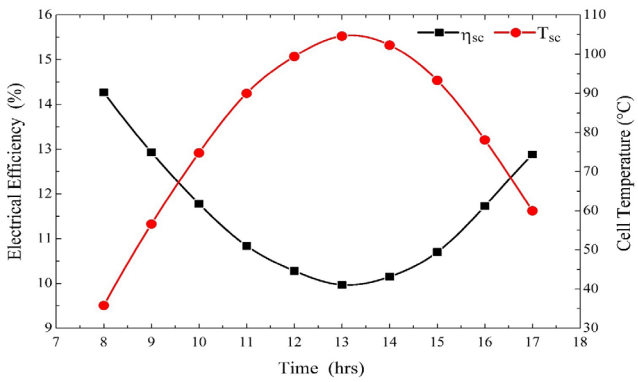

Fig. 5. Hourly variation of electrical efficiency of solar module covering the PVT system for corresponding cell temperature.

correspond to temperature variations of key components across 24 h. The highest temperature difference between basin and glass for both systems is found to occur between 12:00 h to 16:00 h with peak temperature difference of 18.9°C and 14.7°C for active natural and conventional system at 13:00 h respectively. It is found to result in peak hourly yield for both the systems also to occur during same period with peak yield obtained at 14:00 h as illustrated in Fig. 7. This highlights the critical role of higher basin and glass temperature difference for obtaining a higher yield for both systems.

4.5. Comparison of daily hourly yield variation

A comparison of the hourly yield of the conventional solar still and the proposed active natural still is presented in Fig. 7. The hourly yield of the proposed active natural still is significantly higher than the conventional still during sunshine hours of 8:00 h to 17:00 h. Also, the total yield of 4.9 kg/d for proposed active natural circulation system is found to be 88.4% higher than the total yield of 2.6 kg/d for conventional still. The high-temperature operation [14] of CPC systems integrated to still and natural circulation of water in the basin results in higher distillate yield for proposed active natural circulation system as compared to the conventional system throughout the day.

4.6. Comparison of instantaneous thermal efficiency variation

A comparison of variation in instantaneous thermal efficiency of proposed active natural still against conventional still is presented in Fig. 8. The comparison period under consideration is sunshine hours between 8:00 h to 17:00 h. The instantaneous thermal efficiency for conventional still is found to be higher than the proposed active still throughout the day. At the start of the day at 8:00 h, the instantaneous thermal efficiency value of the order of 4.3% is obtained for conventional still against 1.4% for proposed active still. A continuous rise in instantaneous thermal efficiency value for both the stills is observed till the end of the sunshine period at 17:00 h.

With decline in incident radiation after 13:00 h, high yield output corresponding to the reduced instantaneous solar input is obtained towards evening, hence the peak instantaneous thermal efficiency for both the stills is found to occur at 17:00 h. With peak instantaneous thermal efficiency value

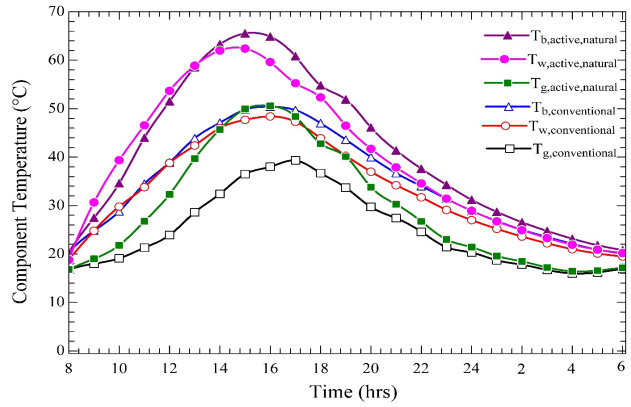

Fig. 6. Hourly variation of component temperature for conventional and active natural solar still.

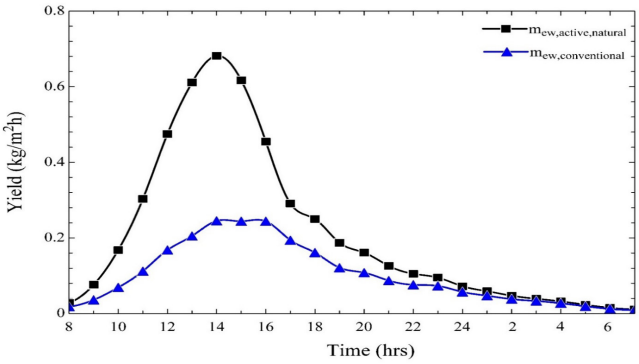

Fig. 7. Daily hourly yield variation for conventional and active natural solar still.

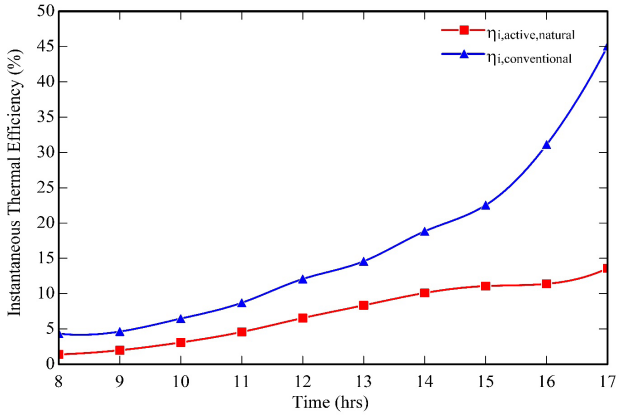

Fig. 8. Instantaneous thermal efficiency variation for conventional and active natural solar still.

of 13.6% at 17:00 h, the proposed active still is 69.8% less efficient than the conventional still with 45.1% instantaneous thermal efficiency value. The conventional still is found to exhibit a comparatively higher increment in instantaneous thermal efficiency value after 13:00 h. The total area receiving the incident radiation for proposed active still is 5.2 times the area of conventional still. The smaller total glass area of conventional still compared to large total glass area of proposed active still intercepting the radiation. This can be credited to a sharper rise in instantaneous thermal efficiency value corresponding to a smaller change in incident radiation for conventional still. Larger solar interception area along with higher operational temperature leading to higher top and bottom losses together can be credited to a lower instantaneous efficiency trend for proposed active still.

The overall thermal efficiency calculated for 24 h for conventional still was found to be 24.2% against 9.8% for proposed active still. Compared to proposed active still, the conventional still offers a higher instantaneous and overall thermal efficiency but smaller value of hourly and total daily yield.

5. Conclusions

The following key findings were made by the analysis:

1. The PVT- CPC integrated active solar still under natural circulation was found to produce 4.9 kg of distilled water per day, that is 88.4% higher yield than the conventional still.
2. The instantaneous thermal efficiency value for the conventional system was found to be higher than that of the proposed active still throughout the day. The peak instantaneous thermal efficiency values for conventional and proposed active still were found to be 45.1% and 13.6% respectively, both occurring at 17:00 h.
3. The overall thermal efficiency value for conventional and proposed active still was calculated for 24 h. The conventional still was found to be 146.9% more efficient than proposed active still.
4. The proposed active still with 5.2 times larger area intercepting the incident radiation exhibited considerably higher yield than conventional still throughout the day and is better suited for conditions where yield is the first priority compared to floor space.
5. In case of proposed active solar still, apart from enhanced daily yield, electrical power is the added benefit which can be used to drive motor for forced mode or any other suitable application.

Symbols

A_b	—	Basin area
A_{apvt}	—	Area of aperture for PVT-CPC collector (m^2)
A_{rpvt}	—	Area of receiver of PVT-CPC collector (m^2)
b_r	—	Width of receiver (m)
b_a	—	Width of aperture area (m)
C_w	—	Specific heat of Water (J/kg K)
F'	—	Factor of efficiency for PVT collector
h_i	—	Coefficient of heat transfer for space between glazing and absorber surface ($W/m^2 K$)
h'_i	—	Coefficient of heat transfer of bottom of PVT-CPC and ambient ($W/m^2 K$)

h_o — Coefficient of heat transfer from top surface of PVT-CPC (W/m² K)
h_{absf} — Coefficient of heat transfer from PVT-CPC absorber surface to water (W/m² K)
I_u — Useful solar radiation intensity (W/m²)
$I_{(t)}$ — Total Incident solar radiation intensity (W/m²)
K_{gc} — Thermal conductivity of glass cover (W/m K)
K_{im} — Thermal conductivity of the bottom insulation (W/m K)
K_{abs} — Thermal conductivity of absorber surface (W/m K)
D_g — Thickness of glass cover (m)
L_{rpv} — Length of receiver of semitransparent PV module (m)
L_{apv} — Length of aperture of semitransparent PV module (m)
D_{im} — Thickness of bottom insulation (m)
D_{as} — Thickness of absorber surface (m)
$\dot{m}_w$ — Mass flow rate of fluid (kg/m²)
PF_1 — Penalty factor due to glass cover of semitransparent PV module
PF_2 — Penalty factor due to absorber surface below PV module
PF_c — Penalty factor due to glass covers for collector covered by glazing
$\dot{Q}_{uth,N}$ — The rate of useful thermal energy (W)
T_{amb} — Ambient temperature (°C)
T_{sc} — Cell temperature (°C)
T_b — Basin water temperature in solar still (°C)
T_w — Temperature of water in circulation (°C)
T_{wi} — Inlet temperature of water (°C)
T_{wo} — Outlet temperature of water (°C)
T_{abs} — Surface temperature of absorber in PVT collector (°C)
T_0 — Reference cell temperature for optimum cell efficiency i.e. 25°C
$U_{m,amb}$ — Overall heat loss coefficient from module to ambient (W/m² K)
$U_{g,amb}$ — Overall heat loss coefficient from glazing to ambient (W/m² K)
$U_{sc,amb}$ — Overall heat loss coefficient from cell to ambient (W/m² K)
$U_{sc,abs}$ — Overall heat loss coefficient from cell to absorber surface (W/m² K)
$U_{abs,amb}$ — Overall heat loss coefficient from absorber to ambient (W/m² K)
V — Air velocity (m/s)
$m_{ew,\ conventional}$ — Daily hourly yield per hour for conventional still (kg/h)
$m_{ew,\ active,natural}$ — Daily hourly yield per hour for proposed still (kg/h)

Greek

α — Absorptivity
β — Packing factor
β_0 — Temperature coefficient of efficiency
ρ — Reflectivity
τ — Transmissivity
η — Efficiency
η_i — Instantaneous thermal efficiency
$(\alpha\tau)_{eff}$ — Product of effective absorptivity and transmittivity

Subscripts

amb — Ambient
sc — Solar cell/collector
eff — Effective
f — Fluid
f_i — Inlet fluid
f_o — Outlet fluid
g — Glass
m — Module
abs — Absorber
el — Electrical

References

[1] G.N. Tiwari, Solar Energy: Fundamentals, Design, Modelling and Applications, Narosa Publishing House, India, 2016.
[2] A. Ghobeity, A. Mitsos, Optimal design and operation of desalination systems: New challenges and recent advances, Curr. Opin. Chem. Eng., 6 (2014) 61–68.
[3] A. Giwa, N. Akther, A. Al Housani, S. Haris, S.W. Hasan, Recent advances in humidification dehumidification (HDH) desalination processes: Improved designs and productivity, Renew. Sustain. Energy Rev., 57 (2016) 929–944.
[4] A.B. Pouyfaucon, L. Garcia-Rodriguez, Solar thermal-powered desalination: A viable solution for a potential market, Desalination, 435 (2018) 60–69.
[5] M.A. Abdelkareem, M. El Haj Assad, E.T. Sayed, B. Soudan, Recent progress in the use of renewable energy sources to power water desalination plants, Desalination, 435 (2018) 97–113.
[6] G.N. Tiwari, L. Sahota, Review on the energy and economic efficiencies of passive and active solar distillation systems, Desalination, 401 (2017) 151–179.
[7] G.N. Tiwari, L. Sahota, Advanced Solar Distillation Systems: Basic Principles, Thermal Modeling, and Its Application, Springer Publication, Singapore, 2017.
[8] A.K. Tiwari, G.N. Tiwari, Thermal modeling based on solar fraction and experimental study of the annual and seasonal performance of a single slope passive solar still: The effect of water depths, Desalination, 207 (2007) 184–204.
[9] A.K. Tiwari, G.N. Tiwari, Annual performance analysis and thermal modelling of passive solar still for different inclinations of condensing cover, Int. J. Energy Res., 31 (2007) 1358–1382.
[10] A.K. Tiwari, G.N. Tiwari, Evaluating the performance of single slope passive solar still for different slope of cover and water depths by thermal modeling: In moderate climatic condition, Sol. Energy, (2006) 1613–1621.
[11] A.K. Tiwari, G.N. Tiwari, Effect of water depths on heat and mass transfer in a passive solar still: in summer climatic condition, Desalination, 195 (2006) 78–94.
[12] A.K. Tiwari, G.N. Tiwari, Effect of inclination of condensing cover and water depth in solar still for maximum yield: in winter climatic condition, Energy Convers. Resour., (2005) 395–407.
[13] H.N. Panchal, S. Patel, An extensive review on different design and climatic parameters to increase distillate output of solar still, Renew. Sustain. Energy Rev., 69 (2016) 750–758.
[14] T. Arunkumar, R. Jayaprakash, A. Ahsan, D. Denkenberger, M.S. Okundamiya, Effect of water and air flow on concentric tubular solar water desalting system, Appl. Energy, 103 (2013) 109–115.

[15] H. Mousa, M.A. Arabi, Desalination and hot water production using solar still enhanced by external solar collector, Desal. Water Treat., 51 (2013) 1296–1301.
[16] J.M. Pearce, D.C. Denkenberger, Numerical simulation of the direct application of compound parabolic concentrators to a single effect basin solar still, in Proceedings of the 2006 International Conference of Solar Cooking and Food Processing, 118 (2006).
[17] E. Deniz, Energy and exergy analysis of flat plate solar collector-assisted active solar distillation system, Desal. Water Treat., 57 (2016) 24313–24321.
[18] R. Poblete, G. Salihoglu, N.K. Salihoglu, Investigation of the factors influencing the efficiency of a solar still combined with a solar collector, 57 (2016) 29082–29091.
[19] T. Arunkumar, R. Velraj, D.C. Denkenberger, R. Sathyamurthy, K.V. Kumar, A. Ahsan, Productivity enhancements of compound parabolic concentrator tubular solar stills, Renew. Energy, 88 (2016) 391–400.
[20] R. Tripathi, G.N. Tiwari, Energetic and exergetic analysis of N partially covered photovoltaic thermal-compound parabolic concentrator (PVT-CPC) collectors connected in series, Sol. Energy, 137 (2016) 441–451.
[21] G.N. Tiwari, M. Meraj, M.E. Khan, R.K. Mishra, V. Garg, Improved Hottel-Whillier-Bliss equation for N-photovoltaic thermal-compound parabolic concentrator (N-PVT-CPC) collector, Sol. Energy, 166 (2018) 203–212.
[22] D.L. Evans, Simplified method for predicting photovoltaic array output, Sol. Energy, 27 (1981) 555–560.
[23] T. Schott, Operational temperatures of PV modules-A theoretical and experimental approach, In: Proceedings of 6th Photovoltaic Sol. Energy Conf., (1985) 392–396.
[24] G.N. Tiwari, M. Meraj, M.E. Khan, Exergy analysis of N-photovoltaic thermal-compound parabolic concentrator (N-PVT-CPC) collector for constant collection temperature for vapor absorption refrigeration (VAR) system, Sol. Energy, 173 (2018) 1032–1042.
[25] J.-A. Jiang, J.-C. Wang, K.-C. Kuo, Y.-L. Su, J.-C. Shieh, J.-J. Chou, Analysis of the junction temperature and thermal characteristics of photovoltaic modules under various operation conditions, Energy, 44 (2012) 292–301.

Appendix A

The following unknown terms were used in presented thermal modeling.

$$U_{sc,amb}=\left[\frac{L_g}{K_g}+\frac{1}{h_0}\right]^{-1};U_{sc,abs}=\left[\frac{L_g}{K_g}+\frac{1}{h_i}\right]^{-1};$$

$$h_2=5.7+3.8V/\mathrm{m^2K};\ V=1\ \mathrm{m/s};$$

$$h_b=\left[\frac{L_i}{K_i}+\frac{1}{h_i}\right]^{-1};$$

$$U_{abs,amb}=\left[\frac{1}{U_{sc,amb}}+\frac{1}{U_{sc,abs}}\right]^{-1}+\left[\frac{1}{h'_i}+\frac{1}{h_{pf}}+\frac{L_i}{K_i}\right]^{-1}$$

$$h'_i=2.8+3V'W/m^2K;\mathrm{V'}=1m/s;$$

$$U_{L1}=\frac{U_{tc,p}U_{tc,a}}{U_{tc,p}+U_{tc,a}};U_{L2}=U_{L1}+U_{abs,amb};U_{Lm}=\frac{h_{pf}U_{L2}}{F'^{h_{pf}}+U_{L2}};$$

$$PF_1=\frac{U_{tc,p}}{U_{tc,p}+U_{tc,a}};PF_2=\frac{h_{pf}}{F'h_{pf}+U_{L2}};$$

$$A_{rpv}=b_rL_{rpvt};A_{apvt}=b_aL_{apvt};$$

$$C=\frac{A_{apvt}}{A_{rpvt}}$$

$$(\alpha\tau)_{1,eff}=(\alpha_{sc}-\eta_{sc})\rho\tau_g\beta C;$$

$$(\alpha\tau)_{2,eff}=\rho\alpha_{abs}\tau_g{}^2(1-\beta_{sc})C;$$

$$(\alpha\tau)_{m,eff}=\left[PF_1(\alpha\tau)_{1,eff}+(\alpha\tau)_{2,eff}\right];$$

$$(UA)_{eff}=A_{rpvt}U_{lpvt};$$

$$(\alpha\tau)_{eff}=A_{rpvt}PF_2(\alpha\tau)_{meff};$$